Mon. Not. R. Astron. Soc. **000**, 000–000 (0000) Printed 13 January 2011 (MN LATEX style file v2.2)

The Magnetic and Metallic Degenerate G77-50

J. Farihi[1], P. Dufour[2], R. Napiwotzki[3],and D. Koester[4]
[1]*Department of Physics & Astronomy, University of Leicester, Leicester LE1 7RH, UK; jf123@star.le.ac.uk*
[2]*Département de Physique, Université de Montréal, Montréal, QC H3C 3J7, Canada*
[3]*Centre for Astrophysics Research, University of Hertfordshire, Hatfield AL10 9AB, UK*
[4]*Institut für Theoretische Physik und Astrophysik, University of Kiel, 24098 Kiel, Germany*

ABSTRACT
An accumulation of multi-epoch, high-resolution, optical spectra reveal that the nearby star G77-50 is a very cool DAZ white dwarf externally polluted by Mg, Fe, Al, Ca, and possibly Na, Cr, Mn. The metallic and hydrogen absorption features all exhibit multiple components consistent with Zeeman splitting in a $B \approx 120$ kG magnetic field. Ultraviolet through infrared photometry combined with trigonometric parallaxes yield $T_{\rm eff} = 5310$ K, $M = 0.60\,M_{\odot}$, and a cooling age of 5.2 Gyr. The space velocity of the white dwarf suggests possible membership in the Galactic thick disk, consistent with an estimated total age of 8.6 Gyr. G77-50 is spectrally similar to G165-7 and LHS 2534; these three cool white dwarfs comprise a small group exhibiting both metals and magnetism.

The photospheric metals indicate accretion of rocky debris similar to that contained in asteroids, but the cooling age implies a remnant planetary system should be stable. A possibility for G77-50 and similarly old, polluted white dwarfs is a recent stellar encounter that dynamically rejuvenated the system from the outside-in. Metal abundance measurements for these cooler white dwarfs have the potential to distinguish material originating in outer region planetesimals injected via fly-by. If common envelope evolution can generate magnetic fields in white dwarfs, then G77-50 and its classmates may have cannibalized an inner giant planet during prior evolution, with their metals originating in terrestrial bodies formed further out. Although speculative, this scenario can be ruled out if terrestrial planet formation is prohibited in systems where a giant planet has migrated to the inner region nominally engulfed during the post-main sequence.

Key words: circumstellar matter— planetary systems— stars: abundances— stars: evolution— stars: magnetic fields— white dwarfs

1 INTRODUCTION

Metal-enriched white dwarfs have experienced a resurgence of interest coinciding roughly with the launch of *Spitzer*. Beginning with the landmark study of Zuckerman et al. (2003), evidence has gradually accumulated supporting a picture whereby most, if not all cool, metal-lined white dwarfs obtain their photospheric heavy elements via rocky bodies similar in composition and in mass to large Solar System asteroids (Farihi et al. 2010a; Jura 2006). Data substantiating this picture comes primarily from *Spitzer* photometric detections of infrared excess indicating circumstellar dust orbiting within the Roche limit of a substantial fraction of metal-contaminated white dwarfs (Farihi et al. 2009; von Hippel et al. 2007), and via mid-infrared spectroscopy of the disk material, revealing silicate minerals (primarily olivines) associated with rocky planet formation (Jura et al. 2009a; Reach et al. 2005).

A powerful example of the scientific potential inherent in these stars is the spectacularly polluted white dwarf GD 362 (Kawka & Vennes 2005; Gianninas et al. 2004). This system shows remarkable infrared excess emission from closely orbiting dust, reprocessing over 3% of the incident stellar flux and exhibiting perhaps the strongest silicate emission feature associated with *any* mature star (Jura et al. 2007). The optical spectrum of GD 362 displays 15 elements heavier than helium in an abundance pattern mimicking the Earth-Moon system (Zuckerman et al. 2007). The convection zone of the star has been enriched, at a bare minimum, by the equivalent of a 240 km asteroid, and possibly by a body as massive as Callisto or Mars, with promising evidence for internal water (Jura et al. 2009b). Thus, white dwarfs enable unique insights into terrestrial planet formation around intermediate mass stars by providing data that can be obtained no other way; a lower mass limit to and

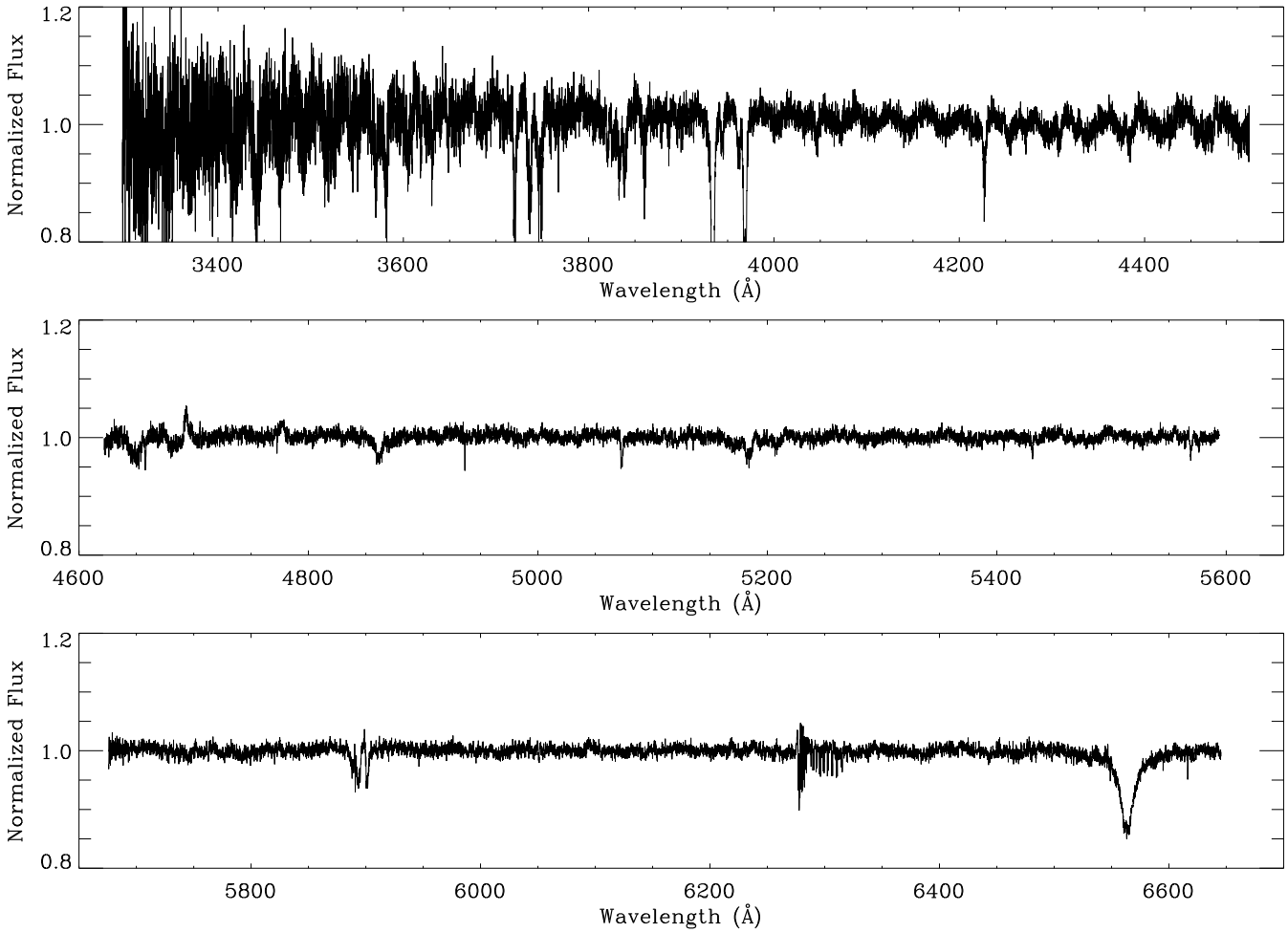

Figure 1. The normalized and coadded UVES spectrum of G77-50, rebinned onto a grid with spacing 0.1Å.The quasi-periodic pattern prominent at shorter wavelengths is due to a light path difference between the flat-field lamp and the sky; this interference is not fully correctable, especially at high S/N. Several previously unidentified metal absorption features are evident, including lines of Mg, Fe, Al, Ca, and perhaps Na, Cr, Mn. Hβ is detected for the first time in a very cool white dwarf. There are a large number of weak lines present in the spectrum whose authenticity is uncertain. The features in the green arm below 4700Å and those in the red arm near 5900Å and 6250Å are detector artifact and telluric absorption residuals (Table 1).

the bulk chemical composition of extrasolar rocky, minor or possibly major planets.

This paper investigates the spectral, kinematical, and atmospheric properties of the white dwarf WD 0322−019 (G77-50). The star has been known as a very cool and metal-lined degenerate for over 35 years (Hintzen & Strittmatter 1974), but was only recently found to exhibit split Ca II H and K absorption lines under high-resolution spectroscopy (Zuckerman et al. 2003). Despite similar, high-resolution spectroscopic observations of several hundred white dwarfs (Koester et al. 2009; Voss et al. 2007), including the detection of a few dozen with Ca II K absorption features (Koester et al. 2005; Zuckerman et al. 2003), only G77-50 and possibly LTT 8381 display evidence for Zeeman-split metallic lines. The observational program and scientific motivation are described in §2, while the spectroscopic analysis, photospheric abundances, and stellar properties are derived in §3. The discussion of the results is contained in §4, where potential origins for the metals and magnetism in G77-50 and related objects are explored in some detail.

2 OBSERVATIONS & DATA

2.1 Echelle Spectroscopy

G77-50 was observed a total of 24 times between 2008 October 4 and November 25 at Cerro Paranal with the 8.2 m Very Large Telescope Unit 2 using the Ultraviolet and Visual Echelle Spectrograph (UVES; Dekker et al. 2000). Spectroscopy was performed over the two detectors covering wavelengths from 3200 Å to 6650 Å using a standard dichroic configuration with $\lambda_c = 3900/5640$ Å, resulting in two narrow gaps in spectral coverage near 4550 and 5650 Å. A slit width of $1\farcs0$ was employed with 2×2 binning, resulting in a nominal resolving power of $R \approx 40\,000$ in both the UV-Blue and Red arms of the instrument. The observations were taken at random intervals that were broadly logarithmic in temporal spacing, with each dataset consisting of two consecutive 900 s exposures. The featureless white dwarf WD 0000−345 (LHS 1008) was observed as a spectral standard on 2008 October 8 using an identical instrumental setup.

Table 1. Notable Features in the Coadded UVES Spectrum of G77-50

Wavelength (Å)	Absorbing Element	Wavelength (Å)	Absorbing Element
3441	Fe I	3934	Ca II
3570	Fe I	3944	Al I
3582	Fe I	3962	Al I
3619	Fe I	3968	Ca II
3631	Fe I	4227	Ca I
3648	Fe I	4600−4700	...
3720	Fe I	4775	...
3735	Fe I	4861	H I
3749	Fe I	5073	...
3758	Fe I	5183	Mg I
3767	Fe I	5890	Na I
3820	Fe I	5900	...
3832	Mg I	6250−6350	...
3838	Mg I	6563	H I
3860	Fe I		

Note. Owing to magnetism, the line centers cannot be determined accurately and the wavelengths given are approximate or laboratory values. In some regions, many lines of Fe I contribute to a single, complex feature but only one wavelength is listed for simplicity. Those features without a corresponding element are due (in part or in whole) to detector artifacts or telluric absorption residuals.

The echelle data were processed with the UVES pipeline version 4.3.0, including cosmic ray masking, flat fielding, wavelength calibration, order merging, and distilled using optimal aperture extraction. Raw spectra produced in this manner had signal-to-noise (S/N) ratios that fell between 16 and 22 at 5000Å. The spectral standard data were interpolated in wavelength to match the solution for the science target and smoothed by 121 pixels (3.5 to 4.0Å). The science target was divided by the spectral standard and the resulting spectrum was multiplied by an appropriate temperature blackbody to achieve a relative flux calibration.

The 2008 UVES dataset was supplemented by two archival UVES observations of G77-50 taken for the SPY survey in 2000 (Napiwotzki et al. 2003), and fully reduced Keck HIRES spectra obtained in 1999 and 1998 (Zuckerman et al. 2003). After correcting for heliocentric velocity at the time of individual exposures, a master spectrum was constructed from the normalized coaddition of all 26 UVES spectra. The resulting spectrum has a bin width of 0.1Å, which increases the S/N, while reducing the original resolution to approximately match the decrease resulting from the wavelength shifts observed in the Ca II H and K lines (see §3). This spectrum is displayed in Figure 1, while Table 1 lists prominent stellar features and non-stellar artifacts.

3 SPECTROSCOPIC ANALYSIS & SYSTEM PARAMETERS

G77-50 is listed as a binary suspect in Bergeron et al. (1997) based on the shape of its Hα absorption feature and the lack of a trigonometric parallax distance at that time. Seeming to confirm this hypothesis, Zuckerman et al. (2003) reported the white dwarf as binary based on what appeared to be double lines of Ca II H and K with large velocity separations, and possible changes in these velocities between two epochs of observation. On the basis of this sound interpretation, the original aim of the UVES program reported here was to obtain the orbital period and mass ratio of the putative binary by measuring and monitoring the velocities of the Ca II H and K line components. A typical, individual UVES spectrum of G77-50 is shown in the top panel of Figure 2 and reveals the seemingly double Ca II features first detected by Zuckerman et al. (2003).

Table 2. Ca II H and K-line Velocity Measurements for G77-50

HJD−2 400 000 (d)	V_- (km s^{-1})	V_+ (km s^{-1})	Instrument
51158.87475	-43.79 ± 1.45	$+82.10 \pm 1.83$	HIRES
51404.10902	-51.36 ± 3.11	$+99.77 \pm 3.61$	HIRES
51737.93210	-61.34 ± 5.43	$+94.93 \pm 6.89$	UVES
51740.88365	-50.32 ± 4.75	$+87.94 \pm 3.73$	UVES
54743.71492	-43.26 ± 2.69	$+98.32 \pm 2.32$	UVES
54743.72596	-48.18 ± 2.71	$+92.99 \pm 2.21$	UVES
54743.73782	-46.78 ± 2.78	$+96.59 \pm 3.60$	UVES
54743.74887	-48.55 ± 2.61	$+91.46 \pm 3.16$	UVES
54743.81040	-50.28 ± 2.87	$+91.03 \pm 2.64$	UVES
54743.82149	-49.51 ± 2.15	$+86.41 \pm 2.90$	UVES
54744.73366	-50.01 ± 1.79	$+89.36 \pm 1.82$	UVES
54744.74471	-47.93 ± 2.43	$+91.32 \pm 2.41$	UVES
54744.83545	-51.48 ± 1.99	$+89.90 \pm 2.40$	UVES
54744.84656	-45.99 ± 2.04	$+87.58 \pm 1.80$	UVES
54747.69594	-54.15 ± 2.32	$+97.44 \pm 2.32$	UVES
54747.70700	-56.27 ± 2.51	$+94.08 \pm 2.27$	UVES
54749.65500	-54.65 ± 4.22	$+88.54 \pm 2.95$	UVES
54749.66605	-53.95 ± 2.97	$+93.02 \pm 2.77$	UVES
54750.66219	-58.50 ± 1.87	$+91.74 \pm 1.96$	UVES
54750.67321	-52.67 ± 2.09	$+92.08 \pm 2.26$	UVES
54759.63148	-46.90 ± 3.15	$+81.53 \pm 3.08$	UVES
54759.64259	-38.68 ± 2.40	$+94.38 \pm 2.40$	UVES
54760.73176	-44.87 ± 2.32	$+79.17 \pm 2.55$	UVES
54760.74281	-42.05 ± 3.26	$+85.12 \pm 3.15$	UVES
54767.68013	-44.27 ± 2.07	$+76.15 \pm 2.15$	UVES
54767.69118	-38.95 ± 1.70	$+82.10 \pm 1.35$	UVES
54795.63988	-41.59 ± 2.30	$+81.30 \pm 2.55$	UVES
54795.65095	-37.12 ± 1.92	$+79.29 \pm 1.82$	UVES

3.1 Analysis and Interpretation of the 'Double' Calcium Lines

3.1.1 Morphological Origins and Issues

Initially, the two components seen in the Ca II H and K lines of each UVES spectrum were treated as originating in distinct stellar constituents in a spatially-unresolved binary. New measurements taken in 2008 (MJD > 54000) were combined with velocities obtained via identical analysis of archival UVES and Keck HIRES data to determine an orbital period. Each major component of the Ca II features were simultaneously fitted by a Gaussian plus a Lorentzian line profile with the programme FITSB2 (Napiwotzki et al. 2004). The parameters of the line profiles were determined simultaneously for all spectra, i.e. assuming a constant line strength and shape (more on this below). The component velocities thus obtained are listed in Table 2. If the measured variations in the line shifts were due to binarity, then

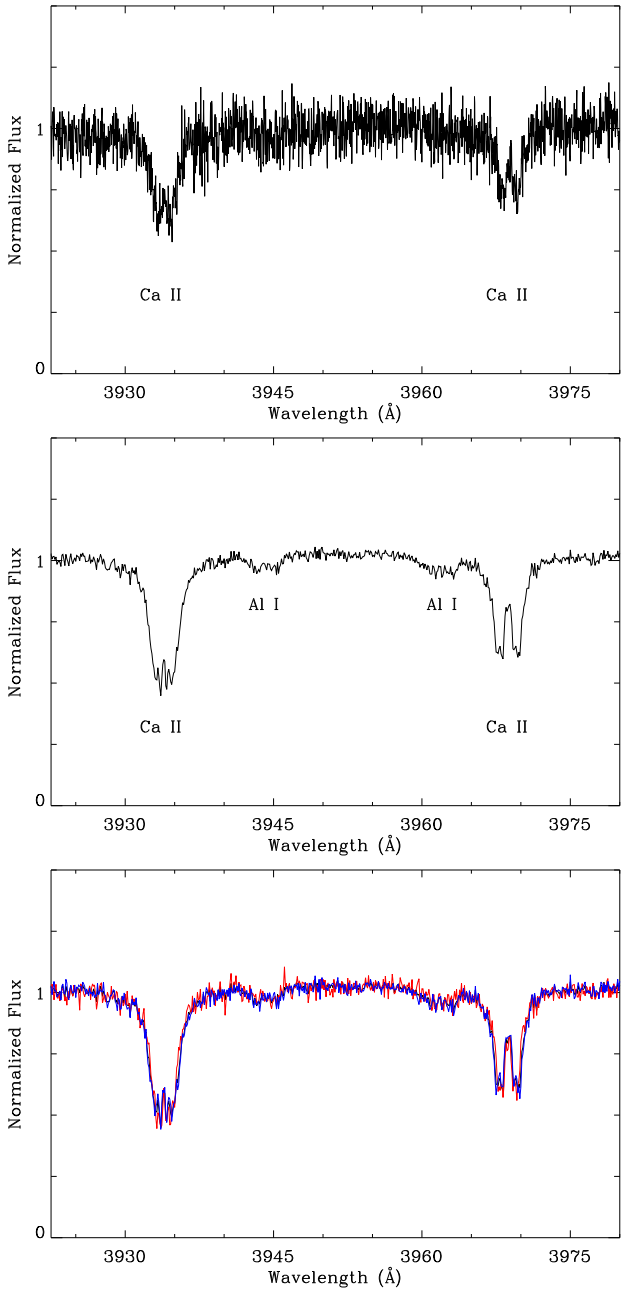

Figure 2. *Upper*: An example of an unbinned, single UVES spectrum of G77-50 in the Ca II H and K region. Each individual exposure exhibits these double-peaked, metal absorption lines. *Middle*: The same region in the combined spectrum of all 26 UVES exposures. In this deep spectrum, broad absorption features due to Al I are revealed. *Lower*: In red and blue, the two coadded spectral subsets discussed in §3.1.1 are shown, plotted on top of the master spectrum in black.

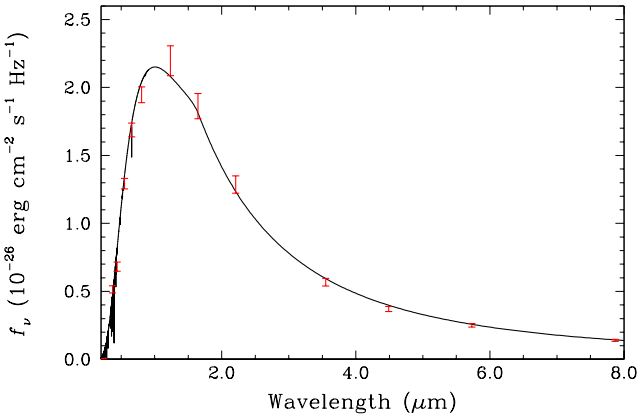

Figure 3. Spectral energy distribution of G77-50 as revealed by *GALEX* (Martin et al. 2005), *UBVRIJHK* (McCook & Sion 1999; Bergeron et al. 1997), and *Spitzer* IRAC (Farihi et al. 2008) photometry . The red error bars plot the observational data, and the black solid line is the stellar atmosphere model with parameters listed in Table 3

each stellar component should exhibit both red- and blue-shifted lines over time. Under this assumption, a sinusoidal period of almost exactly 2.0 d can be found within the line velocity data.

However, if the observed changes in the Ca II H and K line components are the result of orbital motion in two components of a binary, then the resulting velocity amplitudes predict an essentially equal mass system. One can then estimate the radii and masses of the components based on two independent trigonometric parallaxes for G77-50; Smart et al. (2003) report $\pi = 59.5 \pm 3.2$ mas or $d = 16.8^{+1.0}_{-0.9}$ pc, while the US Naval Observatory (H. Harris 2010, private communication) measure $\pi = 58.02 \pm 0.44$ mas or $d = 17.2^{+0.2}_{-0.1}$ pc. Taking the latter value by virtue of its smaller error, the predicted absolute magnitude of each equally luminous component would be $M_V = 15.7$ mag. At a nominal effective temperature of 5200 K (Bergeron et al. 1997), this corresponds to 0.9 $M_\odot$ components.

While this possibility is exciting as the total mass would then easily exceed the Chandrasekhar limit, it also leads to a major inconsistency. The ultraviolet through infrared photometric energy distribution of G77-50 is consistent with a single effective temperature (Figure 3), and thus if the system were binary, the stars would be twins to all limits of observation, in temperature, in mass-radius, and also in metal abundance as the Ca II H and K line components are equally strong. However, the profiles of the Hα line in individual UVES spectra are found to be inconsistent with hydrogen-rich white dwarf models with $\log g > 8.1$; high surface gravities fail to reproduce the observed line. The results of the Hα line fitting are consistent with a single, cool white dwarf at $d = 17.2$ pc as determined by trigonometric parallax.

Based on the discrepancies described above, the master spectrum was constructed as detailed in §2 and carefully examined by eye. The individual spectra exhibit only Hα, Ca II H and K prominently, but the combination of all UVES exposures yields a S/N $\approx$ 100 spectrum with many additional metal features and weak Hβ absorption. Importantly, all detected features in the coadded spectrum show evidence for multiple components, indicating the presence of a weak magnetic field.

Given the spread in line component velocities as shown in Table 2, it is possible the lines will be smeared or otherwise diluted by the coaddition of all individual UVES spectra. To investigate the magnitude of this effect, the distribution of line velocities was searched for subgroups with similar values, whose coaddition might result in better line

sensitivity. Two groupings were identified and these spectral subsets were coadded as above: 7 spectra with V_+ in the range $75.5 - 84.5\,\mathrm{km\,s^{-1}}$ and 15 spectra with V_+ in the range $87.5 - 95.5\,\mathrm{km\,s^{-1}}$. A section of these two spectra are shown in the lower panel of Figure 2 along with the master spectrum. The noise level of the subset spectra are increased compared to the master dataset, and there is no significant change in the shape or depth of the Ca II H and K lines, nor the weak Al I lines. [It is noteworthy that the moderately strong Ca I line shown in the lower right panel of Figure 4 compares favorably in sharpness to both the non-magnetic and Zeeman-split models (§3.2).]

3.1.2 Constraints on Line Variability and Rotation

In this alternative picture, the velocity variation observed in the Ca II H and K line components is most likely due to stellar rotation. Assuming the star is not seen pole-on, the line of sight changes resulting from rotation span a (narrow) range of surface magnetic field strengths, and these induce changes in the strength of the observed Zeeman splitting.

In order to search for periodicities in the wavelength shifts seen in the split H and K lines, a periodogram analysis was performed for 1) $\Delta V = |V_+ - V_-|$ and 2) V_+ and V_- independently. The first approach is adopted here, but the second yielded very similar results. A best fit is found for $P = 29.84579\,\mathrm{d}$ and $\chi^2 = 25.9$, down from 280.5 when assuming constant line velocities, and thus indicating a high statistical significance of the variable solution. The phase-folded velocity differences confirm a good quality fit with $\chi^2_{\mathrm{red}} = 1.04$, with a number of somewhat poorer fits are present in the period range $28 - 33\,\mathrm{d}$. Two distinct solutions cannot be ruled out completely: $1.0311\,\mathrm{d}$ ($\chi^2 = 33.8$) and $0.011333\,\mathrm{d}$ ($\chi^2 = 35.6$). The latter period is suspect as it is similar to the length of the individual UVES exposures, while periods near $1.0\,\mathrm{d}$ are always dubious, and hence $29.85\,\mathrm{d}$ is the most likely solution. For a dipolar field configuration, half a rotation will produce a full cycle in the line velocities; if the long period solution is real, the white dwarf would be a slow rotator.

The relatively strong Ca II features were examined for variation in strength over time within the UVES dataset. Measuring reliable equivalent widths for these blended lines was not possible, but the area swept out beneath the continuum was examined as a proxy. Roughly half the feature strengths for both the H and K lines are found in a single, 0.5σ-width peak, with all other measurements sitting below this peak, including some negative (i.e. unphysical) values. Based on this analysis, the individual spectra do not have sufficient S/N to meaningfully constrain variability in the observed line strengths.

3.2 Stellar Parameters and Abundances

When first studied, Hα was not detected in the optical spectrum of G77-50 and the white dwarf was typed as DG in the classification scheme of the period (Hintzen & Strittmatter 1974). Subsequently, Greenstein (1986) detected Hα and Sion et al. (1990) typed the star in the modern spectral classification as a DZA white dwarf; strongest lines are metallic, weaker line(s) of hydrogen. It is not clear whether feature strength should be determined by depth or equivalent width (E. M. Sion 2010, private communication), but in the case of G77-50, a DAZ classification is readily arguable as its atmosphere is hydrogen-rich, with trace metals.

Table 3. Stellar and Kinematical Parameters of G77-50

T_{eff}	$5310 \pm 100\,\mathrm{K}$
$\log\, g\,(\mathrm{cm\,s^{-2}})$	8.05 ± 0.01
M	$0.60 \pm 0.01\,M_\odot$
M_{ms}	$1.4 \pm 0.2\,M_\odot$
t_{cool}	$5.2 \pm 0.1\,\mathrm{Gyr}$
t_{ms}	$3.4 \pm 1.3\,\mathrm{Gyr}$
t_{tot}	$8.6 \pm 1.3\,\mathrm{Gyr}$
π_{trig}	$58.02 \pm 0.44\,\mathrm{mas}$
(μ_α, μ_δ)	$(241, -877)\,\mathrm{mas\,yr^{-1}}$
$z_{\mathrm{g}}c$	$31.5\,\mathrm{km\,s^{-1}}$
v_{rad}	$-11.2\,\mathrm{km\,s^{-1}}$
v_{tan}	$74.3\,\mathrm{km\,s^{-1}}$
v	$75.1\,\mathrm{km\,s^{-1}}$
(U, V, W)	$(-44.2, -60.5, -5.0)\,\mathrm{km\,s^{-1}}$

As a first step, T_{eff} and $\log g$ are obtained by re-fitting existing $BVRIJHK$ photometric data with the latest pure hydrogen model atmosphere grid and using the new parallax measurement, following the method of Bergeron et al. (1997). From this, an effective temperature of $5310 \pm 100\,\mathrm{K}$ and a surface gravity of $\log g = 8.05 \pm 0.01$ are obtained, corresponding to $0.60 \pm 0.01\,M_\odot$ and a cooling age of $5.2 \pm 0.1\,\mathrm{Gyr}$. Figure 3 plots the global energy distribution obtained with these stellar parameters (listed in Table 3), together with ultraviolet through mid-infrared photometry obtained from both the ground and space. The consistency of the *Spitzer* data with the predicted stellar flux indicates excellent agreement with the model, which was fitted only at shorter wavelengths.

The coadded spectrum of G77-50 indicates the presence of several elements as well as a magnetic field. From the splitting of the various atomic lines, $B \sim 120\,\mathrm{kG}$ is estimated. Such a field is too weak to have an important effect on the thermodynamic structure of the star, and the absorption features are not strong enough to effect the determination of the atmospheric parameters described above. This was verified explicitly *a posteriori* by comparing a pure hydrogen model energy distribution with that of a blanketed model that takes into account the presence of all the heavy elements at the derived abundances. Hence, it is safe to use the above atmospheric parameters for the detailed abundance analysis presented below. It is, however, necessary to include the effect of Zeeman splitting in synthetic spectra calculations to obtain accurate heavy element abundances. As a first order approximation, magnetic line splitting is explicitly included in the synthetic spectrum calculation by assuming the linear Zeeman effect in a constant magnetic field of 120 kG over the surface of the star.

In the presence of a weak magnetic field, an atomic level with total angular momentum J splits into $2J+1$ levels with magnetic quantum number $m = -J, ..., +J$. For each line, all transitions were calculated between the upper and lower levels that are allowed by the selection rule ($m_u - m_l = 0$, +1, -1). Each transition is then shifted by

$$\Delta\lambda = 4.67 \times 10^{-13}\ \lambda_0^2\ B\ (g_l m_l - g_u m_u) \qquad (1)$$

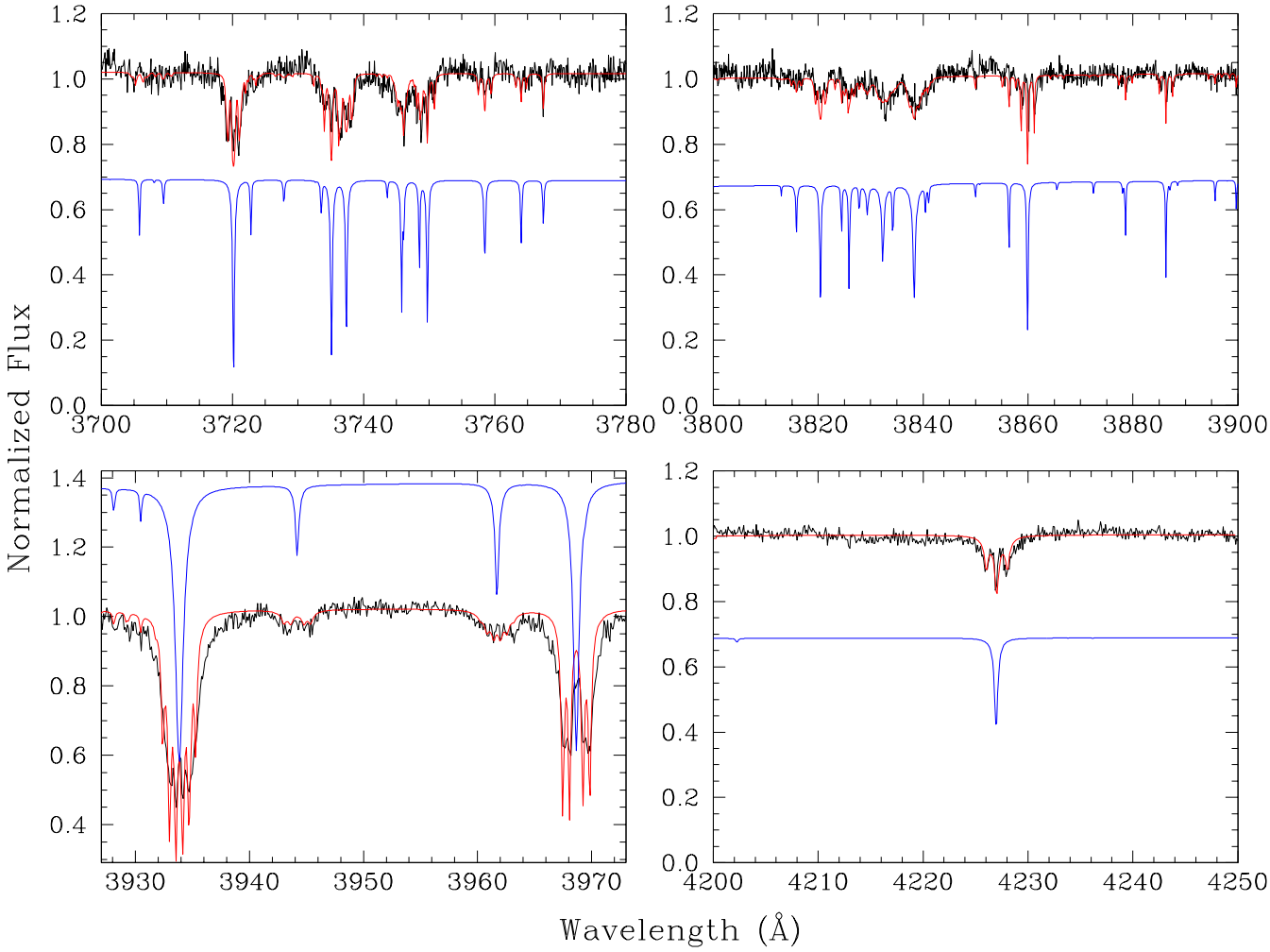

Figure 4. The combined UVES spectrum of G77-50 is shown in black and the best-fit model in red. Vertically offset from the data, the same best-fit, but non-magnetic model is shown in blue for line identification. The following wavelengths correspond to their non-magnetic positions. *Upper left*: All Fe I lines. *Upper right*: Fe I lines and Mg I (3832,3838 Å). *Lower left*: Ca II H & K, Al I (3944,3962 Å), and Fe I (near 3930 Å). *Lower right*: Ca I.

where g is the Landé factor, B the magnetic field strength in G, m the magnetic quantum number of the level and λ_0 the central wavelength of the line in Å. In the few cases where the Landé factor is not given in the VALD[1] line list, the term designation is used to compute the Landé factor under the L-S coupling approximation, i.e.

$$g = 1 + \frac{J(J+1) + S(S+1) - L(L+1)}{2J(J+1)} \qquad (2)$$

The relative strengths of the π, σ ($\Delta m = 0, \pm 1$ respectively) components are calculated according to Sobel'Man (1973).

For the fixed value of $T_{\rm eff}$ and log g determined above, a grid of synthetic, magnetic spectra is then calculated for each of the strongly-detected metals, as well as for more uncertain elements. The grids typically cover an abundance range from $\log[n({\rm Z})/n({\rm H})] = -8.0$ to -11.0 in steps of 0.5 dex. Next the abundance of each element is determined by fitting the various observed lines using a similar method to that described in Dufour et al. (2005). The final adopted abundance of an element is taken as an average of all the fitted features, and these are listed in Table 4. Finally, a synthetic spectrum including all the elements is calculated with the nominal abundances and plotted over the observed spectrum in Figure 4. In order to facilitate the line identification of the various spectral features, a non-magnetic spectrum was also calculated with the same final metal abundances.

Despite the simplicity of using a constant 120 kG field geometry for the synthetic spectrum calculations, the fits are remarkably good. Small discrepancies exist (e.g., in the wings and depth of the strong H & K lines), that are probably an indication that the field strength varies slightly over the surface. It should be noted that the master, coadded spectrum represents an average taken at various, random rotation phases. Synthetic spectrum calculations using a more realistic (dipolar) magnetic field geometry, and a suitable average over the rotation period, would probably provide a better fit to the Ca II lines, but it is unlikely that such an effort would affect the derived abundances significantly.

To find possible weak features arising from elements other than Mg, Fe, Al, and Ca, a synthetic spectrum was

[1] http://vald.astro.univie.ac.at

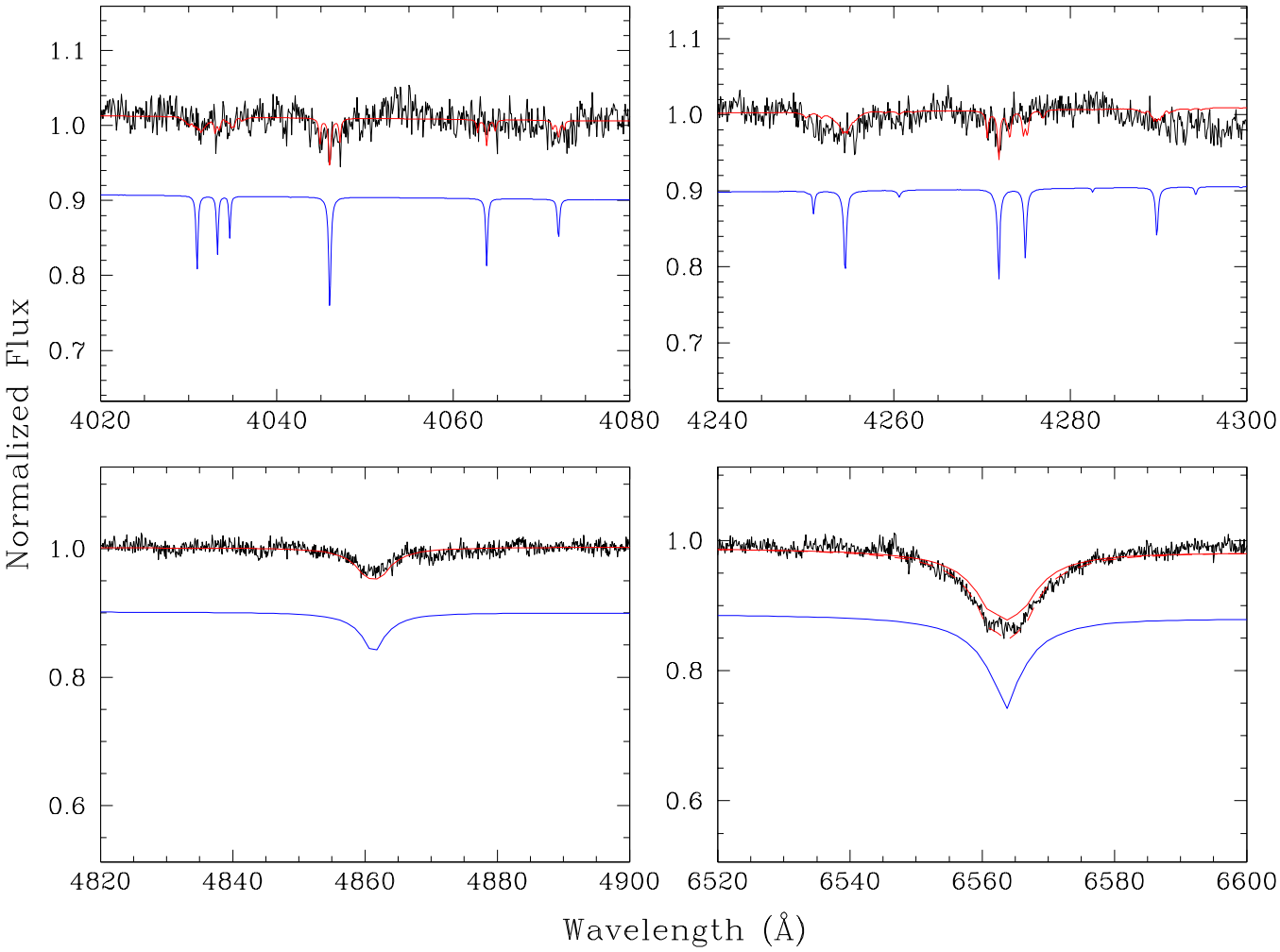

Figure 4 – *continued Upper left*: Uncertain Mn I features (4030,4033,4034 Å), and Fe I lines. *Upper right*: Uncertain Cr I features (4254,4274 Å), and Fe I lines. *Lower panels*: Hydrogen Balmer lines α, β. The dashed line in the Hα panel corresponds to a model 100 K warmer than that used for the paper analysis (§3.3).

calculated with all elements up to Ni in abundances somewhat higher than their chondritic ratios (Lodders 2003) relative to the observed Ca in G77-50. This enhanced spectrum was laid over the coadded spectrum and a careful search was done by eye, allowing identification of the strongest possible features for additional elements as well as upper limits. The search revealed the possible presence of very weak features of Mn I (4030,4033,4034 Å) and Cr I (4254,4274 Å; see Figure 4). However, the putative features are only slightly above the noise level of the spectrum and thus these elements are considered uncertain.

The Na I D doublet region also contains features (Figure 1), but caution is warranted as this portion of the spectrum is contaminated by detector artifacts which significantly complicate the analysis. A careful examination of all 26 individual UVES spectra indicates that the 5890 Å line is real and thus Na is likely detected in this star. Unfortunately, the energy levels involved in these transitions are too close for the linear Zeeman approximation in a 120 kG magnetic field, and the Paschen-Back regime is appropriate. Hence, the position and strength of the lines cannot be matched with the calculations presented here, and an accurate analysis of Na in this star is best left for future work with cleaner data. Nevertheless, a rough Na abundance is obtained by matching the depth of the observed feature with the Zeeman approximation model, but interpretations based on this element should be avoided.

Lastly, the synthetic Hα profile, appropriately split by a 120 kG magnetic field, is found to be slightly weaker than the observed line, whose strength depends sensitively on the effective temperature of the star. A model with a temperature increased by 100 K produces a line profile that matches the observations well (Figure 4), and falls within the effective temperature uncertainty obtained from the fit to the photometric energy distribution.

3.3 Stellar Kinematics

Armed with an average, total velocity shift of $\gamma = +20.3\,\mathrm{km\,s^{-1}}$ from the median of all the Ca II line centers in Table 2, a mass-radius constrained by trigonometric parallax, the stellar radial velocity of G77-50 can be disentangled from its gravitational redshift. The approximation

Table 4. Metal Abundances and Masses in G77-50

Element	$\log[n(\mathrm{Z})/n(\mathrm{H})]$	M_z (10^{20} g)	t_diff (10^5 yr)
Na†	−9.1	0.25	3.76
Mg	−8.3	1.62	3.85
Al	−9.2	0.20	3.72
Ca	−9.8	0.08	2.78
Cr‡	−9.9	0.08	2.49
Mn‡	−10.3	0.03	2.36
Fe	−8.7	1.31	2.33
Total	−8.0	3.57	

†Abundance uncertain.

‡Presence of this element is uncertain.

Note. Errors are 0.2 dex

$$z_\mathrm{g} \approx \frac{GM}{c^2 R} \tag{3}$$

is valid for white dwarfs. For a star of $0.60\,M_\odot$ and $\log g = 8.05$, the radius is $R = 0.0121\,R_\odot$ and $v_\mathrm{g} = 31.5\,\mathrm{km\,s^{-1}}$. Thus the radial velocity of the binary system is $v_\mathrm{rad} = \gamma - v_\mathrm{g} = -11.2\,\mathrm{km\,s^{-1}}$. Table 3 lists the resulting three dimensional space motion for G77-50 incorporating the above radial velocity and its observed proper motion (Zacharias et al. 2010). While the velocities are not extreme, the V component lags behind the rotation of the Galaxy by $60\,\mathrm{km\,s^{-1}}$, indicating the white dwarf belongs to the old thin or thick disk population (Pauli et al. 2006).

A total age for the white dwarf can be estimated in the following way. Taking the average and standard deviation of three independent initial-to-final mass relations (Williams et al. 2009; Kalirai et al. 2008; Dobbie et al. 2006), the main-sequence progenitor of G77-50 had a likely mass of $1.4 \pm 0.2\,M_\odot$. Main-sequence lifetimes for stars in this mass range are obtained from the analytical formulae of Hurley et al. (2000), and added to the cooling age of the white dwarf. This results in a total system age of 8.6 ± 1.3 Gyr for G77-50, a range consistent with thick disk membership, although not conclusively.

4 ORIGIN OF METALS AND MAGNETISM

Some of the material presented in this section is necessarily speculative, and are first attempts to understand how a star such as G77-50 came to possess its somewhat unusual characteristics. It should be the case that near-future theoretical and empirical investigations will be able to test these ideas more rigorously.

4.1 Nature of the Photospheric Metals

Metal diffusion timescales and convection zone parameters for G77-50 were calculated using a complete model atmosphere with the parameters and heavy element abundances from the preceding analysis in the outer layers. This was continued to the bottom of the convection zone using pure hydrogen Koester (2009). Table 4 lists the relevant lifetimes for all the metals detected or suspected in G77-50. The total mass of the mixing layers in G77-50 is found to be 1.23×10^{27} g, and can be combined with the photospheric abundances to obtain the current mass of each heavy element within the star. As the metals continuously sink, these calculations yield the *minimum* mass of each accreted metal, and are listed in Table 4. The total mass of metals residing in the star is 3.57×10^{20} g and equivalent to that contained in a 65 km diameter body of density $2.5\,\mathrm{g\,cm^{-3}}$; the highest mass of heavy elements yet inferred within a hydrogen-rich white dwarf.

Owing to its very cool effective temperature, G77-50 possesses a sizable convection zone on par with those intrinsic to helium-rich white dwarfs (Koester 2009). Thus, the star has a commensurately long diffusion timescale for heavy elements; e.g. 280,000 yr for Ca. In this and other respects, G77-50 is characteristic of the coolest metal-rich white dwarfs. It has modest metal abundances, with $\log[n(\mathrm{Z})/n(\mathrm{H})] < -8.5$ for all but Mg, a relatively low time-averaged accretion rate of $3.7 \times 10^7\,\mathrm{g\,s^{-1}}$ for all clearly detected and suspected heavy elements, and a lack of infrared excess as measured with *Spitzer* IRAC photometry (Farihi et al. 2009, 2008), indicating a dearth or absence of dust in its immediate circumstellar environment.

The relatively old white dwarf has a total space velocity of $75\,\mathrm{km\,s^{-1}}$ and its current location is 17.2 pc from the Sun. At this speed, the star travels nearly $77\,\mathrm{pc\,Myr^{-1}}$ and may be passing through the relatively interstellar matter-deficient Local Bubble (Redfield & Linsky 2008; Welsh et al. 1999), its metal content decaying from a past event within a dense region of gas and dust. Within a period just over 1 Myr, G77-50 could have been outside the Local Bubble, and its metal abundances would have decayed by a factor between 20 and 100, depending on the element. With roughly 2×10^{22} g of atmospheric metals in this picture, how dense an interstellar region is necessary to account for the accretion in such a manner? For interstellar heavy elements typically contained in dust particles, the accretion rate onto a star is (Farihi et al. 2010a):

$$\dot{M}_\mathrm{z} = \frac{\pi G M R \rho_\infty}{s} \left(\frac{T_\mathrm{eff}}{T_\mathrm{ev}}\right)^2 \tag{4}$$

where M and R are the stellar mass and radius, $s = \sqrt{v^2 + {c_s}^2}$ is the space velocity v in the supersonic regime ($v \gg c_s$) appropriate for G77-50, and T_ev is the evaporation temperature of the dust grains. Conservatively estimating that dust evaporates at 1000 K, the minimum density required to deposit 2×10^{22} g of metal in the star over a typical sinking timescale of 3×10^5 yr is $1600\,\mathrm{cm^{-3}}$. While such densities exist in molecular clouds, the space velocity of G77-50 requires continuous accretion over a distance of 30 pc in order that sufficient material is captured. This scenario is unlikely; one of the nearest and largest cloud complexes, the Orion Nebula is only about 8 pc in diameter.

Alternatively, the metals in the star were accreted from its circumstellar environment and were originally contained within remnant planetary bodies rich in heavy elements. The detection of both Al and Ca in the star supports a scenario in which the metals originated in a refractory-rich source such as a rocky, minor or major planet. This possibility is likely based on the weight of evidence favoring circumstellar accretion among the observed population of single, cool, and metal-enriched white dwarfs (Zuckerman et al. 2010; Farihi et al. 2010a). In this scenario, the photospheric metals in G77-50 were delivered by one or more rocky planetary

Table 5. Metal Ratios in G77-50 and Other Polluted White Dwarfs with Al

Star	Name	Mg/Fe	Al/Fe	Ca/Fe	Disk?
0322−019	G77-50	2.9	0.31	0.08	−
		1.2†	0.14†	0.06†	
	solar	1.2	0.10	0.07	−
0208+096	G74-7	1.0	0.08	0.11	−
0300−013	GD 40	1.7	0.21	0.40	+
1633+433	G180-63	2.1	0.14	0.18	−
1729+371	GD 362	0.5	0.18	0.26	+

†At the end of an *assumed* accretion event 0.5 Myr prior.

Note. The three middle columns list the relative number abundances. Metal ratios for other white dwarfs with Al detections are taken from the literature (Klein et al. 2010; Zuckerman et al. 2007, 2003; Lodders 2003).

bodies passing close enough to the white dwarf to become tidally destroyed or otherwise accreted (Jura 2003).

For a prior pollution event, the current metal-to-metal ratios have been altered from the accreted values, via the individual heavy element sinking timescales. Table 5 lists the photospheric abundance ratios, relative to Fe, for the four heavy elements confidently identified in G77-50. Notably, both Mg/Fe and Al/Fe appear enhanced relative to solar values and to the stars with circumstellar dust; precisely as expected in a declining phase because Fe sinks most rapidly. Interestingly, Ca/Fe is nearly solar, yet down by a factor of a few compared with the stars currently accreting from disks. Under the questionable assumption that the accreted abundances were close to solar, then the photospheric pollution halted roughly 0.5 Myr ago. In all likelihood, the accretion epoch for G77-50 ended within the last few to several diffusion timescales, no longer than a few Myr ago. Events older than 3 Myr ago imply an Fe-dominated ($M_{\rm Fe}/M_{\rm z} \geqslant 94\%$) parent body more massive than Pluto.

4.2 A Late Instability Near 5 Gyr

Again, G77-50 epitomizes the older and cooler, $T_{\rm eff} < 9000$ K metal-rich white dwarfs: something weighty has occurred recently in these Gyr old, presumably stable systems. Generally, the timescale for a planetary system to dynamically settle – pre- or post-main sequence – should be 100 Myr (Debes & Sigurdsson 2002), and thus a catastrophic event at Gyr epochs is not expected for G77-50 and similar white dwarfs. Dual planet interactions will occur during this short period, if they occur at all, but instabilities among three (or more) planets may occur on longer timescales, as hypothesized for the period of Late Heavy Bombardment in the Solar System (Gomes et al. 2005).

Following Debes & Sigurdsson (2002) and Chambers et al. (1996) for the simple case of three $0.001\,M_{\odot}$ planets, one can calculate system architectures that give rise to an instability timescale of 5.2 Gyr during the white dwarf evolutionary stage. Taking initial and final stellar masses to be 1.8 and $0.6\,M_{\odot}$ produces an (adiabatic) orbital expansion factor of 3 between the main and post-main sequence phases. For an innermost planet now located at 10 AU, the outer planets would be near 30 and 157 AU, with original – and presumably metastable – semimajor axes of 3.3, 10, and 52 AU (Debes & Sigurdsson 2002). In general, for all layouts that keep the innermost planet safely outside the stellar photosphere ($a_1 > 2$ AU) during the asymptotic giant branch, the planets must be spaced such that $a_2/a_1 \gtrsim 3$ and $a_3/a_2 \gtrsim 10$. Thus, the onset of instability at Gyr timescales requires a somewhat finely-tuned, increasingly wide planet spacing.

An alternate way in which an old and stable planetary system might be efficiently agitated is a stellar encounter. Though rare, at the cooling age and space velocity of G77-50, it can be shown that at least one fly-by is consistent with theoretical expectations. Dynamically, the number of stellar encounters per unit time, within a distance D of a star is given by (García-Sánchez et al. 1999):

$$N = \pi D^2 v_* \rho_* \tag{5}$$

where v_* is the space velocity of the white dwarf relative to passing stars, and ρ_* is the local density of stars and stellar systems. From *Hipparcos* data, the velocity dispersion of stars within 2 kpc of the Sun and $|b| > 30\,^{\circ}$ varies between 22 and 44 km s^{-1} depending on spectral type (Mignard 2000). Later type stars tend to be kinematically more stirred as they represent, on the whole, relatively older populations. And because the most abundant stars in the Galaxy are K and M dwarfs, these relatively fast moving stars are the objects for which encounters are most likely. Taking 40 km s^{-1} for a typical field star and the 75 km s^{-1} space velocity of G77-50 yields $v_* = 85$ km s^{-1}. The local space density of stars is 0.081 pc^{-3} (T. Henry 2010, private communication; Henry et al. 2006)[2], and Equation 5 gives $N = 22$ Myr^{-1} for encounters within 1 pc. For close fly-bys that might significantly impact the outer regions of a planetary system, take $D \leqslant 1000$ AU and then $N = 0.5$ Gyr^{-1}. If correct, and such an encounter is 50% probable within each 0.5 Gyr window, then it is 99.9% likely that G77-50 has suffered at least one such stellar encounter within its 5.2 Gyr cooling history.

An encounter could disturb a Kuiper Belt analog originally orbiting at a few to several tens of AU, but now residing at one to a few hundred AU owing to mass lost during the post-main sequence. Large objects such as Sedna, whose mass is similar to Ceres, can readily be perturbed into high eccentricity orbits by a stellar encounter, thus sending outer planetesimals towards the inner system (Kenyon & Bromley 2004). While chances are tiny that any single, distant body could be flung directly within the tidal disruption radius of the white dwarf, the perturbation of many bodies (i.e. a significant fraction of a surviving population) could result in their capture and further scattering within the inner system (Debes & Sigurdsson 2002).

A potential hurdle for this hypothesis is the total available mass that survives heating during the giant phases at these orbital distances. Out to roughly 100 AU, objects composed of pure water ice and up to 100 km in diameter should sublimate completely (Jura 2004; Stern et al. 1990), but the overall effect on realistic bodies of heterogenous chemical composition is unknown. For example, some models predict that subsurface volatiles should be protected by superior

[2] Statistics of the solar neighborhood are continually updated at http://www.recons.org

layers of non-volatile material such as silicates (Jura & Xu 2010). Studies of Kuiper Belt analogs in the post-main sequence may reveal the overall impact of sublimation and constrain the total mass that survives to the white dwarf stage (Bonsor & Wyatt 2010).

In contrast, Oort cloud analogs will not be destroyed via heating but are prone to dynamical evaporation in the post-main sequence if the stellar mass loss is asymmetric (Parriott & Alcock 1998). At tens of thousands of AU, stellar encounters can be frequent over Gyr timescales typical of very cool white dwarfs such as G77-50. These events should strip away some portion of any Oort-like cloud, but also perturb another fraction onto eccentric orbits overlapping with the inner system. If such cold, outer planetesimal belts are ultimately responsible for some fraction of metal-polluted white dwarfs, then a large deposition of volatile elements would be expected, but has not yet been observed (Zuckerman et al. 2007; Jura 2006).

The subset of older and cooler metal-rich white dwarfs that G77-50 represents are a relatively high velocity group of stars, typically with $T > 50\,\mathrm{km\,s^{-1}}$ (Aannestad et al. 1993), and the above exercise can be broadly applied to Gyr age white dwarfs with metals. Thus, stellar encounters have the potential to make ancient planetary systems dynamically young for a brief period, and may account for the population of very cool DAZ and DZ stars, of which vMa 2 is the prototype.

4.3 Weak Magnetism

In the favored model for cool, metal-rich white dwarfs, a planetary system has survived post-main sequence evolution (Debes & Sigurdsson 2002). Instabilities drive rocky planetary bodies such as asteroids into close approach with the compact star, where they become tidally- or otherwise destroyed and are sometimes observed as dust disks (Jura 2003). For the high eccentricity orbits necessary for the (eventual) delivery of metals onto the surface of the star, conventional sized planets are the most efficient perturbers. In this picture, an otherwise-replete planetary system persists at metal-enriched white dwarfs, likely truncated near the maximum radius of the asymptotic giant progenitor star.

Based on precision radial velocity planet searches, 10.5% of FGK dwarfs with masses in the range $0.7-1.3\,M_{\odot}$ host gas giant planets within 3 AU (Cumming et al. 2008). Due to the finite time period over which these searches have been carried out, most of these giant planets orbit within 1 AU, and a decent fraction orbit close to their host star (the so-called hot jupiters). Relative to these findings for solar-type stars, giant planets are found more frequently, and with a higher mass distribution, in radial velocity searches of intermediate mass stars. Both Lovis & Mayor (2007) and Johnson et al. (2007) find that planet frequency and planet (minimum) mass scale with stellar host mass, and that the fraction of gas giants orbiting within 3 AU of stars with masses between around 1.5 and $2.0\,M_{\odot}$ is closer to 25% (Bowler et al. 2010). Interestingly, stars with higher masses do not host closely-orbiting giant planets, possibly due to halted orbital migration from rapid inner disk dissipation (Currie 2009), or planet-star gravitational tides (Hansen 2010).

The bulk of giant planets orbiting within a few AU of their host stars will be destroyed during the post-main sequence phases of their host stars. During the first ascent giant branch (RGB), stars with main-sequence masses above $1.0\,M_{\odot}$ expand to around $10-20\,R_{\odot}$, or $0.05-0.10$ AU, sufficient to swallow only the hot planets (Bowler et al. 2010; Villaver & Livio 2009). Depending on which initial-to-final mass relation one uses, the main-sequence progenitor of G77-50 was an early to late F star with a mass between 1.2 and $1.6\,M_{\odot}$. For a $M > 1.3\,M_{\odot}$ progenitor, there is a 25% chance it hosted a giant planet within a few AU, but not a hot planet. In this case, the inner planet would survive the RGB intact but most likely become enveloped during the asymptotic giant branch (AGB), either directly or via tidal forces; a $1.5\,M_{\odot}$ star has a maximum AGB radius near 2.4 AU (Villaver & Livio 2007).

Depending on the mass and angular momentum of an engulfed planet, a common envelope may develop for a time sufficient to generate a magnetic dynamo (Nordhaus et al. 2010; Tout et al. 2008; Siess & Livio 1999b; Regős & Tout 1995). The eventual accretion of the planet onto the stellar core may also result in enhanced mass loss from the giant (Siess & Livio 1999a), producing a white dwarf remnant potentially less massive than predicted by initial-to-final mass relations. If this occurs at the level of $0.05\,M_{\odot}$ in the white dwarf, then the inferred mass of the progenitor star will be biased towards lower, main-sequence masses. In the model of Potter & Tout (2010), the longer the common envelope environment, the larger the magnetic field strength in the resulting white dwarf plus companion merger. This model predicts fields up to 10^7 G in a common envelope lasting roughly 10^4 yr, but with a stellar companion generating the convective motions. Following Potter & Tout (2010) but reducing the companion mass by a factor of 100 (to $10\,M_{\mathrm{J}}$), all else being equal, a magnetic field of 10^5 G is predicted. Interestingly, the surface field of G77-50 is 1.2×10^5 G.

4.4 Possible Planetary System Architecture

In the admittedly speculative picture outlined above, the primordial G77-50 system formed a gas giant that migrated through a disk to an inner orbit. Subsequently and beyond this orbit, additional planets may have formed (Mandell et al. 2007). As in the Solar System and a significant fraction of main-sequence stars (Carpenter et al. 2009; Su et al. 2006), a Kuiper belt analog existed at G77-50, consisting of primordial icy and rocky bodies condensed from the stellar nebula. During post-main sequence evolution, the volatile outer layers of these planetesimals were lost by evaporation and radiation pressure, leaving behind objects with non-volatile surfaces and intact cores (Bonsor & Wyatt 2010; Jura & Xu 2010).

In order that a stellar encounter repopulate the inner, circumstellar regions around any star, sizable planets must exist there to trap or further scatter injected bodies. Such captured planetesimals are vulnerable to perturbations via newly established resonances on 100 Myr timescales (Debes & Sigurdsson 2002). From this point forward in time, the eventual pollution of the star by a tidally destroyed planetesimal proceeds as envisioned for metal-rich white dwarfs with cooling ages less than 0.5 Gyr (Farihi et al. 2009; Jura 2003). If the stellar encounter hypothesis applies to G77-50 and other very cool, polluted white dwarfs, then the

atmospheric metals may be a reflection of the rocky remains of primitive, outer system planetesimals rather than Solar System asteroid analogs. As such, they would have a composition distinct from objects that formed at higher temperatures in the inner system, presumably including a higher concentration of volatile elements.

Testing this hypothesis may be difficult. While cooler white dwarfs have lower atmospheric opacities and hence detection of their heavy elements is less challenging, there are two complications. The main difficulty is that the coolest DAZ and DZ stars are not amenable to ultraviolet spectroscopy, which is the ideal region to search for volatiles (or any element) in low abundance. For example, trace amounts of atmospheric carbon are only seen in the optical spectra of cool, helium-rich white dwarfs, and only at abundances $\log[n(\mathrm{C})/n(\mathrm{He})] > -7$ (Dufour et al. 2005). If C/Fe = 8.3 in G77-50 as in chondrites, then it would have $\log[n(\mathrm{C})/n(\mathrm{H})] = -7.8$ and be undetectable in this manner. Also, it is not clear what fraction of volatile material would remain after heating and ablation during the post-main sequence (Jura 2006).

An additional complication is that it is difficult to constrain the epoch of accretion in these cooler, metal-polluted stars. Observationally, it is rare that cool DAZ or DZ have dust disks, and this may be the result of a significant reduction in the ratio of disk lifetime to cooling age. The observed abundances can be used to constrain the epoch of accretion, but this is fundamentally biased towards the composition of Solar System objects and may not accurately reflect those of extrasolar planetary bodies. This latter concern may be partially alleviated in the growing number of DZ stars being found in the Sloan Digital Sky Survey (Dufour et al. 2007); follow up of these stars will better constrain the relative frequency of disks at older, metal-enriched stars and their abundances will hopefully provide clues to the nature of the polluting bodies.

5 CONCLUSIONS

The cool white dwarf G77-50 is found to be simultaneously metal-contaminated and magnetic. A hypothesis that may account for both properties is an evolved planetary system. While highly uncertain, it is possible that G165-7 (Dufour et al. 2006) and LHS 2534 (Reid et al. 2001) acquired their magnetic fields and photospheric metals in a manner analogous to G77-50. In this tentative picture, an inner giant planet was swallowed by the post-main sequence progenitor, creating a common envelope whose convective motions generated the extant magnetic field. Surviving rocky planetesimals have polluted the star with several refractory metals that are typical major constituents of asteroids and inner Solar System planets (Allègre et al. 1995). However, with a cooling age of 5.2 Gyr, it is difficult to imagine a planetary system architecture with instabilities sustained over such a period. A plausible model is a stellar encounter that perturbs outer planetesimals into the inner system, where planets scatter and trap them with a renewed dynamical potential for close approaches with the white dwarf.

The exact nature of the parent body whose metals currently pollute G77-50 will likely remain uncertain for the foreseeable future. The white dwarf has been observed over a large wavelength range with the two most powerful, high-resolution optical spectrographs currently available, and with the exception of Na, the detections and abundances here are not likely to be improved upon. Furthermore, the effective temperature of the star means that there is little flux to observe with the ultraviolet spectrographs on *HST*. G77-50 and other very cool DAZ and DZ stars will have to await more powerful long wavelength observations with *JWST* or ALMA.

ACKNOWLEDGMENTS

The authors thank the anonymous referee for helpful comments that improved the manuscript. J. Farihi thanks I. N. Reid and B. Zuckerman for sharing their HIRES datasets, and H. Harris (and the USNO) for providing the details of their latest parallax results for G77-50. P. Dufour is a CRAQ postdoctoral fellow. This work is based on observations made with ESO Telescopes at Paranal Observatory under programme 382.D-0804(A).

REFERENCES

Aannestad, P. A., Kenyon, S. J., Hammond, G. L., Sion, E. M. 1993, AJ, 105,1033
Allegre C. J., Poirier J. P.,Humler E., Hofmann A.W. 1995, Earth Planetary Sci. Letters, 4, 515
Bergeron P., Ruiz M. T., Leggett S. K. 1997, ApJS, 108, 339
Bonsor, A., Wyatt, M. 2010, MNRAS, 409, 1631
Bowler, B. P., et al. 2010, ApJ, 709, 396
Carpenter, J. M. et al. 2009, ApJS, 181, 197
Chambers, J. E., Wetherill, G. W., Boss, A. P.1996, Icarus, 119, 261
Cumming, A., Butler, R. P., Marcy, G. W., Vogt, S. S., Wright, J. T., Fischer, D. A. 2008, PASP, 120, 531
Currie, T. 2009, ApJ, 694, L171
Debes J. H., Sigurdsson S. 2002, ApJ, 572, 556
Dekker H., D'Odorico S., Kaufer A., Delabre B., Kotzlowski H. 2000, SPIE, 4008, 534
Dobbie P. D., et al. 2006, MNRAS, 369, 383
Dufour P., Bergeron, P., Fontaine, G. 2005, ApJ, 627, 404
Dufour P., Bergeron P., Schmidt G. D., Liebert J., Harris H. C., Knapp G. R., Anderson Schneider D. P. 2006, ApJ, 651, 1112
Dufour P., et al. 2007, ApJ, 663, 1291
Farihi J., Barstow M. A., Redfield, S., Dufour P., Hambly N. C. 2010a, MNRAS, 404, 2123
Farihi J., Jura M., Lee J. E., Zuckerman B. 2010b, ApJ, 714, 1386
Farihi J., Jura M., Zuckerman B. 2009, ApJ, 694, 805
Farihi J., Zuckerman B., Becklin E. E. 2008, ApJ, 674, 431
Fontaine G., Brassard P., Bergeron P. 2001, PASP, 113, 409
García-Sánchez, J., Preston, R. A., Jones, D. L., Weissman P. R., Lestrade, J. F., Latham, D. W., Stefanik, R. P. 1999, AJ, 117, 1042
Gianninas, A., Dufour, P., Bergeron, P. 2004, ApJ, 617, L57

Gomes, R., Levison, H. F., Tsiganis, K., Morbidelli, A. 2005, /nat, 435, 466
Greenstein J. L. 1986, ApJ, 304, 334
Hansen, B. M. S. 2010, ApJ, 723, 285
Henry, T. J., Jao, W.-C., Subasavage, J. P., Beaulieu, T. D., Ianna, P. A., Costa, E., Méndez, R. A. 2006, AJ, 132, 2360
Hintzen P., Strittmatter P. A. 1974, ApJ, 193, L111
Hurley, J. R., Pols, O. R., Tout, C. A. 2000, MNRAS, 315, 543
Johnson, J. A., Butler, R. P., Marcy, G. W., Fischer, D. A., Vogt, S. S., Wright, J. T., Peek, K. M. G. 2007, ApJ, 670, 833
Jura M. 2003, ApJ, 584, L91
Jura M. 2004, ApJ, 603, 729
Jura, M. 2006, ApJ, 653, 613
Jura M., Farihi J., Zuckerman B. 2009a, AJ, 137, 3191
Jura, M., Farihi, J., Zuckerman, B., Becklin, E. E. 2007, AJ, 133, 1927
Jura M., Muno M. P., Farihi, J., Zuckerman B. 2009b, ApJ, 699 1473
Jura M., Xu, S. 2010, AJ, 140, 1129
Kalirai J. S., Hansen B. M. S., Kelson D. D., Reitzel D. B., Rich R. M., Richer H. B. 2008, ApJ, 676, 594
Kawka, A., Vennes, S. 2005, in ASP Conf. Ser. 334, 14th European Workshop on White Dwarfs, ed. D. Koester, S. Moehler (San Francisco: ASP), 101
Kenyon, S. J., Bromley, B. C. 2004, Nature 432, 598
Klein, B., Jura, M., Koester, D., Zuckerman, B., Melis C. 2010, ApJ, 709, 950
Koester D. 2009, A&A, 498, 517
Koester D., Voss B., Napiwotzki R., Christlieb N., Homeier D., Lisker T., Reimers D., Heber U. 2009, A&A, 505, 441
Koester D., Rollenhagen K., Napiwotzki R., Voss B., Christlieb N., Homeier D., Reimers D. 2005, A&A, 432, 1025
Lovis, C., Mayor, M. 2007, A&A, 472, 657
Lodders, K. 2003, ApJ, 591, 1220
Mandell, A. M., Raymond, S. N., Sigurdsson, S. 2007, ApJ., 660, 823
Martin D. C., et al. 2005, ApJ, 619, L1
McCook G. P., Sion E. M. 1999, ApJS, 121, 1
Mignard, F. 2000, A&A, 354, 522
Napiwotzki R., et al. 2003, Msngr, 112, 25
Napiwotzki et al. 2004, in ASP Conf. Ser. 318, Spectroscopically and Spatially Resolving the Components of the Close Binary Stars, ed. R. W. Hilditch, H. Hensberge, K. Pavlovski (San Francisco: ASP), 402
Nordhaus, J., Wellons, S., Spiegel, D. S., Metzger, B. D., Blackman, E. G. 2010, PNAS, in press (arXiv:1010.1529)
Parriott, J., Alcock, C. 1998, ApJ, 501, 357
Pauli, E. M., Napiwotzki, R., Heber, U., Altmann, M., Odenkirchen, M. 2006, A&A, 447, 173
Potter, A., T., Tout, C. A., 2010, MNRAS, 402, 1072
Reach, W. T., Kuchner, M. J., von Hippel, T., Burrows, A., Mulally, F., Kilic, M., Winget, D. E. 2005, ApJ, 635, L161
Redfield S., Linsky J. L. 2008, ApJ, 673, 283
Regős, E., Tout, C. A. 1995, MNRAS, 273, 146
Reid, I. N., Liebert, J., Schmidt, G. D. 2001, ApJ, 550, L61
Siess, L., Livio, M. 1999a, MNRAS, 304, 925
Siess, L., Livio, M. 1999b, MNRAS, 308, 1133
Sion E. M., Kenyon S. J., Aannestad P. A. 1990, ApJS, 72, 707
Smart R. L., et al. 2003, A&A, 404, 317
Sobel'Man, I. I. 1973, in An Introduction to the Theory of Atomic Spectra, (Oxford: Pergamon Press)
Stern, S. A., Shull, J. M., Brandt, J. C. 1990, Nature, 345, 305
Su, K. Y. L., et al. 2006, ApJ, 653, 675
Tout, C. A., Wickramasinghe, D. T., Liebert, J., Ferrario, L., Pringle, J. E. 2008, MNRAS, 387, 897
Villaver, E., Livio, M. 2007, ApJ, 661, 1201
Villaver, E., Livio, M. 2009, ApJ, 705, L81
von Hippel T., Kuchner M. J., Kilic M., Mullally F., Reach W. T. 2007, ApJ, 662, 544
Voss B., Koester D., Napiwotzki R., Christlieb N., Reimers D. 2007, A&A, 470, 1079
Welsh B. Y., Sfeir D. M., Sirk M. M., Lallement R. 1999, A&A, 352, 308
Williams, K. A., Bolte, M., Koester, D. 2009, ApJ, 693, 355
Zacharias, N., et al. 2010, AJ, 139, 2184
Zuckerman B., Koester D., Melis C., Hansen B. M. S., Jura M. 2007, ApJ, 671, 872
Zuckerman B., Koester D., Reid I. N., Hünsch M. 2003, ApJ, 596, 477
Zuckerman, B., Melis, C., Klein, B., Koester, D., Jura, M. 2010, ApJ, 722, 725